Paper No.
13026

NACE INTERNATIONAL CORROSION Conference & Expo 2019

An Experimental Investigation on the Effect of Salt Concentration on Uniform CO_2 Corrosion

Fazlollah Madani Sani, Bruce Brown, Zineb Belarbi, Srdjan Nesic
Institute for Corrosion and Multiphase Technology, Ohio University
342 W State Street
Athens, Ohio, 45701
USA

ABSTRACT

Hydrocarbon extraction from underground reservoirs is typically accompanied by the production of water as a by-product. Dissolved salts are a general characteristic of produced water. Salt concentration (salinity) in produced water can vary from few milligrams per liter of produced water to about 25 wt.%. Uniform CO_2 corrosion of carbon steel facilities is often a major problem when handling produced water in the oil and gas fields. A very limited amount of research has been conducted on the effect of salt concentration on uniform CO_2 corrosion and those studies did not investigate the subject mechanistically over a large enough range of salt concentration. In this study, the effect of salt concentration on the rate and mechanism of uniform CO_2 corrosion of carbon steel was investigated in a wide range of NaCl concentration from zero to 20 wt.%. Weight loss and electrochemical experiments were performed in a solution saturated with CO_2 (autogenous pH) at 30°C and 1 bar total pressure. The results of weight loss, linear polarization resistance (LPR), and electrochemical impedance spectroscopy (EIS) showed that the corrosion rate decreased with increasing NaCl concentration. Both anodic and cathodic reactions were retarded by higher NaCl concentrations. However, the decrease in the mass transfer of H^+ from the bulk to the surface was identified as the main influential parameter on the decreasing rate of the corrosion process. EIS data indicated that the charge transfer resistance increased and the capacitance of the double layer at the metal/solution interface decreased with increasing NaCl concentration.

Key words: CO_2 corrosion, uniform corrosion, salt concentration, ionic strength, non-ideal solutions, produced water

INTRODUCTION

Water is often produced as a by-product of the production of hydrocarbons from underground reservoirs.[1] The technical term used in the oil and gas industry for this water is “produced water”. On average, for every barrel of crude oil extracted from conventional oil reservoirs, about 7 to 10 barrels of water are produced. This amount is usually lower for gas reservoirs.[2] In addition, the amount of produced water in primary production increases over time when reservoirs age and this amount can be even more if secondary or tertiary recovery methods are used.[3] Dissolved salts are a general characteristic of produced water. It is reported that, in the USA, the concentration of salts in produced water (i.e. salinity) from conventional reservoirs can vary from 1000 (~0.1 wt.%) to 400,000 mg/l (~28 wt.%).[4] Besides salts,

corrosive gases (CO_2 and H_2S) commonly dissolve in produced water, which make the mixture a complex corrosive environment for metallic equipment used throughout the production process.

Internal CO_2 corrosion of carbon steel tubing is one of the important problems encountered in the oil and gas industry.[5] A large body of research exists on this type of corrosion. However, most of this research focused on a salt concentration range of 1 to 3 wt.%, which is much lower than the salt concentrations encountered in the field.[6] There are few studies that have been done on uniform CO_2 corrosion at salt concentrations above 3 wt.%. For example, Fang[5], Zeng *et al.*[7] and Han et al.[8] in similar research reported that CO_2 corrosion rate of carbon steel decreased with increasing salt concentration. On the other hand, Eliyan *et al.*[9,10] and Liu *et al.*[11] reported that the CO_2 corrosion rate of carbon steel showed a maximum with respect to salt concentration. Some of these studies do not cover the whole range of non-ideality (to maximum 10 wt.%), while some others do not address the effect of salt concentration on the corrosion process mechanistically. The advantage of the present work is that it covers a wider range of salt concentration and also includes different methods to mechanistically investigate the effect of salt concentration on uniform CO_2 corrosion.

In this paper, the effect of NaCl concentration on corrosion behavior of carbon steel X65 was investigated by performing weight loss and electrochemical experiments in CO_2-saturated aqueous solution (autogenous pH) at different NaCl concentrations (zero to 20 wt.%), 30°C and 1 bar total pressure. The effect of salt concentration on: pH of solution, the rate of uniform CO_2 corrosion, kinetics of cathodic and anodic reactions, resistance to mass transfer of electroactive species and finally the capacitance of the double layer at the metal/solution interface will be addressed in this research article.

EXPERIMENTAL PROCEDURE

A 2-liter glass cell with a classical three-electrode setup was used for the corrosion experiments.
Figure 1 shows the experimental apparatus. The reference electrode was a silver/silver chloride (Ag/AgCl) electrode. The counter electrode was a platinized titanium mesh with dimensions 20 mm×30 mm. The working electrode (specimen) shown in Figure 1 (B) was a rotating cylinder electrode (RCE) made from API 5L X65 carbon steel with a chemical composition listed in Table 1. The API 5L X65 steel grade is frequently used in oil and gas transmission pipelines.[12]

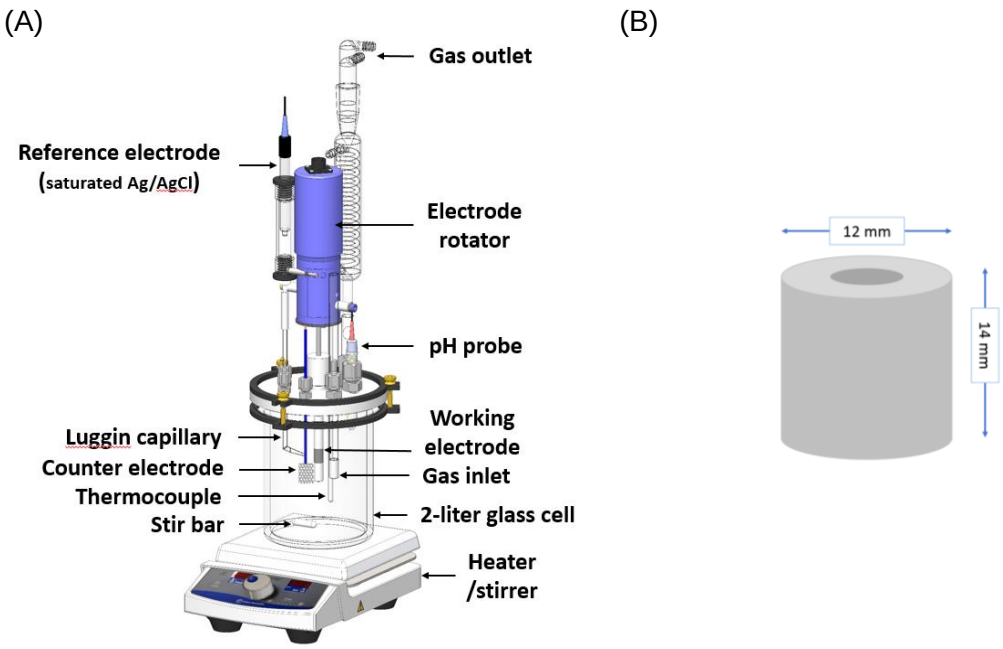

Figure 1: (A) experimental setup; (B) dimensions of the X65 RCE

Table 1: Chemical composition of the experimental material (API 5L X65) (in wt.%)

Al	As	C	Co	Cr	Cu	Mn	Mo	Nb	Ni
0.033	0.015	0.05	0.012	0.150	0.140	1.51	0.160	0.03	0.380
P	**S**	**Sb**	**Si**	**Sn**	**Ti**	**V**	**Zr**	**Fe**	
0.004	<0.001	0.035	0.250	0.012	0.01	0.04	0.004	balance	

Two sets of experiments were conducted in CO_2-saturated aqueous solutions with different NaCl concentrations to investigate the effect of salt concentration on uniform CO_2 corrosion. NaCl was chosen as the experimental salt because it is the major salt present in water produced from conventional hydrocarbon reservoirs.[13] For each experiment, a specified amount of NaCl was added to two liter of double-distilled deionized water in a glass cell. The solution was then sparged with CO_2 for at least 2 h while being stirred. Experiments were done at autogenous pH. Measuring pH correctly in high ionic strength solutions is a big challenge.[14] The pH measurements were done with a double-junction pH probe, which was resistant to Na^+ ion interference.

The specimen was sequentially wet polished with 80-, 240-, 400- and 600-grit abrasive papers. Subsequently, it was ultrasonically degreased with isopropanol for 3 min and dried in cool N_2 gas prior to immersion in the test solution.

In the first set of experiments, the weight loss method was used to measure the corrosion rate of specimen at different NaCl concentrations. The linear polarization resistance (LPR) technique was performed in parallel every 6 h to measure the spontaneous corrosion rate. In addition, spectrophotometric analysis was conducted at the end of each weight loss experiment to measure the concentration of ferrous ion in the solution. Both LPR and $[Fe^{2+}]_{(aq)}$ measurements were used to confirm the weight loss results.

In the second set of experiments, electrochemical impedance spectroscopy (EIS) followed by potentiodynamic polarization (PD) were done to study the effect of salt concentration on the mechanism of uniform CO_2 corrosion. Prior to each electrochemical test, the open circuit potential (OCP) was monitored to ensure a stable potential value (ΔE_{OCP}<2 mV/min). The PD experiments were conducted according to the following steps: perform a cathodic sweep starting from the OCP toward more negative potentials, wait for the OCP to return to its initial value (this takes about 30 min), perform an anodic sweep starting from the OCP to more positive potentials. All electrochemical measurements were conducted using a Gamry potentiostat Reference 600†. Table 2 and Table 3 list the details of conditions and methods used in the experiments.

Table 2: The experimental conditions

Parameter	Description
Specimen surface area (cm^2)	5.4
Temperature (°C)	30 ± 1
CO_2 partial pressure (bar)	0.97
NaCl concentration (wt.%)	**Zero, 0.1, 1, 3, 10 and 20**
pH	Autogenous pH
Stirring speed (rpm)	1000

† Trade name

The average corrosion rate from the weight loss experiments was determined by using the following equation:

$$CR = 87.6\frac{W}{DAT} \quad (1)$$

where, CR is corrosion rate in mm/y, W is mass loss in milligrams, D is density of metal in g/cm^3, A is specimen surface area in cm^2, and T is exposure time in hours.[15] The density of the experimental material was considered 7.87 g/cm^3.

Table 3: Details of the experimental methods

Method	Description
Weight loss	
• Duration (h)	24
• Balance precision (mg)	0.1
Potentiodynamic polarization	
• Potential range (V vs. OCP)	-1.0 to 0.35
• Scan rate (mV/s)	0.5
Linear polarization resistance	
• Potential range (mV vs. OCP)	-5.0 to 5.0
• Scan rate (mV/s)	0.125
• B[1] (mV/dec)	26
Electrochemical impedance spectroscopy	
• Frequency range (Hz)	10,000 to 0.1
• DC voltage (V vs. OCP)	Zero
• Peak to peak amplitude (mV)	10
• Sampling rate (points/decade)	8

RESULTS

pH measurement results

Figure 2 shows the changes in the pH of the solution with respect to NaCl concentration at the beginning and at the end of the weight loss measurements. The pH decreased from about 4.0 at zero wt.% NaCl to about 3.5 at 20 wt.%. When salt concentration is increased in a gas-saturated solution, the solubility of gas decreases; this is called "salting out" effect.[8] Therefore, it is expected to have an increase in pH at higher NaCl concentrations because less CO_2 dissolves in the solution and consequently less carbonic acid is produced. However, the pH of the solution decreased with increasing NaCl concentration, which is due to an increase in the activity coefficient of H^+ ion. The activity coefficient of H^+ ion at different NaCl concentrations was calculated with a water chemistry model built based on Pitzer's equations.[16] Figure 3 shows that the activity coefficient of H^+ (dashed line) increased from unity at zero wt.% NaCl to about 3 at 20 wt.% NaCl, while H^+ concentration first increased for concentrations below 3 wt.% and then decreased. When NaCl is dissolved in water, it alters the short- (intermolecular interactions), middle- (ion/ion and ion/molecule) and long-range (electrostatic interactions) forces among different species in the solution.[17] These variations in the forces change the activity coefficient of dissolved species including H^+. The final pH of the solution was greater than the initial pH at each NaCl concentration because of the release of Fe^{2+} in the solution during the corrosion process.

[1] The B value used in Stern-Geary equation

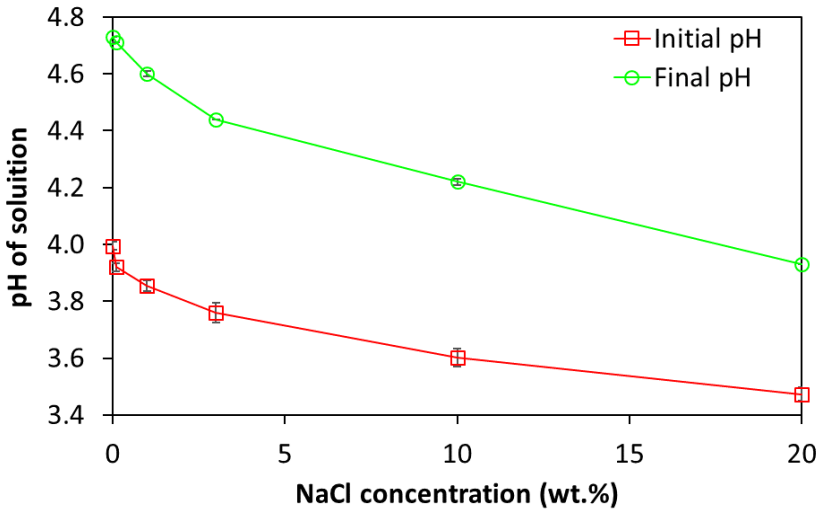

Figure 2: pH of solution vs. NaCl concentration at the beginning and at the end of the weight loss experiments.

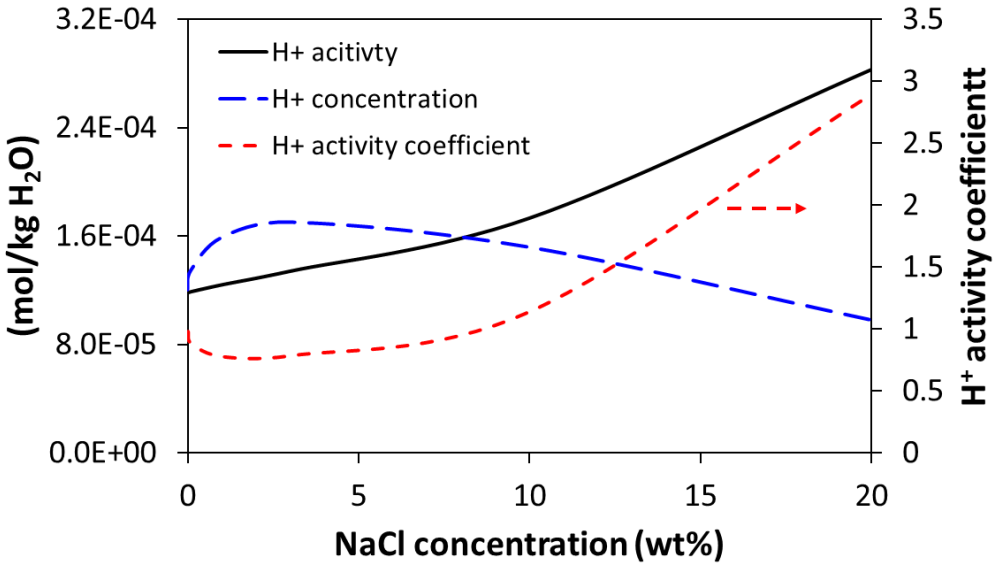

Figure 3: Calculated H^+ activity, concentration and activity coefficient vs. NaCl concentration

Weight loss results

Figure 4 shows the variation in the corrosion rate measured with three methods: weight loss, LPR and $[Fe^{2+}]_{(aq)}$ spectrophotometry as a function of NaCl concentration. The experimental error for the weight loss and $[Fe^{2+}]_{(aq)}$ measurements were satisfactorily small so the error bars in the graphs are overlaid by the data points. A B value of 26 mV/dec was used for the Stern-Geary equation to convert the experimental polarization resistance to the corrosion rate. This value is proven experimentally at Institute for Corrosion and Multiphase Technology to accord the best fit between the LPR and weight loss results. When the rate of the corrosion process is controlled by the rate of mass transfer of corrosive species to the surface ($\beta_c \cong \infty$), which is the case in this study as evident in Figure 5, the Stern-Geary equation can be simplified to $i_{corr} = \frac{\beta_a}{2.3R_P}$ ($B = \frac{\beta_a}{2.3}$). This means that the anodic Tafel slope should be ~60 mV/dec. Similar values were obtained from the potentiodynamic sweeps in Figure 5. Likewise, Zeng *et al.*[7] reported values between 63 to 72 mV/dec. However, the anodic Tafel slope for dissolution of carbon steel in CO_2-containing solution is often reported to be 40 mV/dec.[18–22] In order to compare the LPR and the

weight loss results, the “average LPR” values were calculated by the cumulative trapezoidal integration of the instantaneous LPR corrosion rates.

All three methods showed similar corrosion rates over the entire range of NaCl concentration, implying that the results were reliable. Scanning electron microscopy (SEM) coupled with energy dispersive X-ray analysis (EDX) (data not shown) showed that there was no iron carbonate layer on the surface of the specimen, which was expected because pH was below 4. Therefore, corrosion was uniform and the weight loss results were reliable.

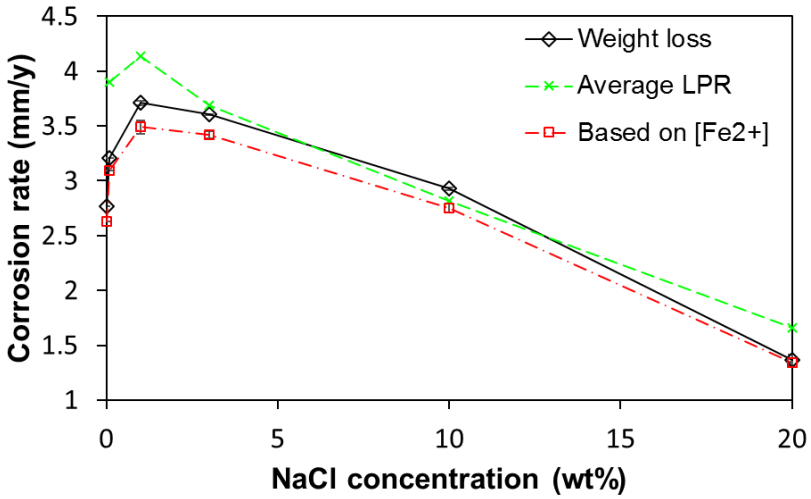

Figure 4: Corrosion rates of X65 RCE at 1000 rpm rotational speed measured with weight loss, LPR and [Fe^{2+}(aq)] spectrophotometry at different NaCl concentrations after 24 h exposure to a solution saturated with CO_2 (autogenous pH) at 30°C and 1 bar total pressure

The corrosion rate increased with an increase in NaCl concentration from zero to 1 wt.% and then decreased by further increase in NaCl concentration. This trend can be justified by looking at the similar trend shown in Figure 3 for the concentration of H^+, which is considered as the main electroactive species for the system under study. Another possible reason for the increase in the corrosion rate at low salt concentrations could be the sudden drop in the solution resistance from 800 Ω at zero wt.% NaCl to 20 Ω at 0.1 wt.% NaCl (data obtained with EIS). However, there is no proof that the solution resistance could directly influence the corrosion rate. The solution resistance becomes important in the presence of an external electrical field, since the electromigration of ions under the influence of the electrical field needs to be considered. However, in a natural corroding condition, there is no electrical field and the electromigration should not influence the corrosion process. The decrease in the corrosion rate with higher NaCl concentration will be discussed in the next sections.

Potentiodynamic polarization results

Effect of salt concentration on cathodic reactions

The effect of NaCl concentration on the potentiodynamic polarization sweeps is shown in Figure 5. The potential values are corrected for the solution resistance (IR drop) in all the sweeps. The corrosion potential (OCP) did not change considerably with NaCl concentration. The key change in the polarization sweeps with increasing NaCl concentration was the decrease in the limiting current. The limiting current depends on the concentration of electroactive species in the bulk, and transport phenomena including density and viscosity of solution, and diffusivity of dissolved species. Eisenberg *et al.*[23] suggested the

following semi-empirical mass transfer correlation for estimating the limiting current at the surface of a cylindrical electrode:

$$i_L = \frac{0.0791 \times n \times F \times V^{0.7}}{{d_{RCE}}^{0.3}} \rho^{0.344} \times \mu^{-0.344} \times D^{0.644} \times c_0 \quad (2)$$

where i_L is limiting current density in A/cm^2, n is valence chage of reacting ion, F is Faraday constant (96485 C/mol), V is linear velocity of the RCE surface in cm/s, d_{RCE} is diameter of RCE in cm, ρ is solution density in g/cm^3, μ is solution viscosity in g/cm-s, D is diffusion coefficient of reacting ion in cm^2/s and c_0 is bulk concentration of reacting ion in mol/cm^3.[23]

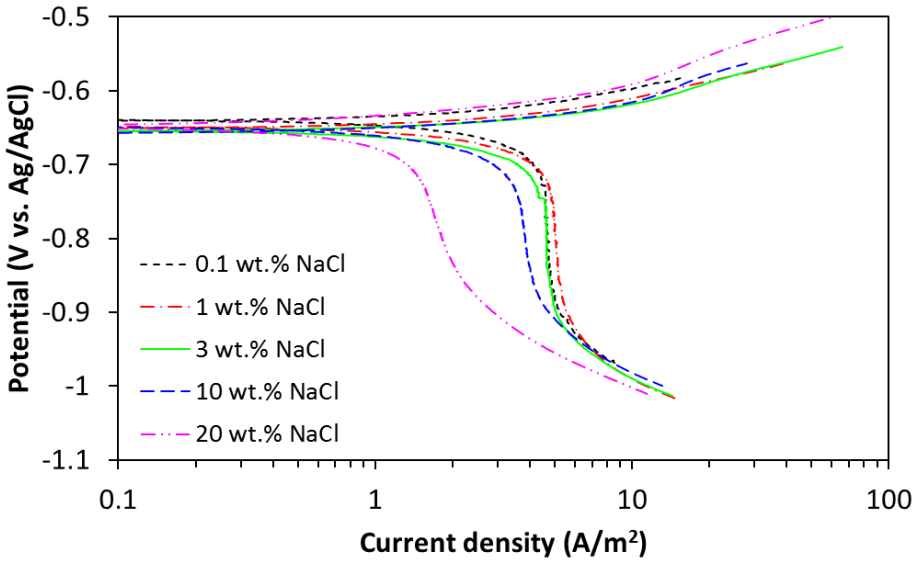

Figure 5: Potentiodynamic polarization sweeps in CO_2-saturated solutions (autogenous pH) with different NaCl concentrations at 30°C, 1 bar total pressure, and 1000 rpm RCE rotational speed

When salt concentration is increased in a solution, the density and viscosity of the solution increase, while the diffusion coefficient of dissolved species decreases. Density and viscosity have opposite exponent signs in Equation (2). It can be assumed that their effects on the limiting current density cancel each other out. This is proven to be true by modeling the effect of each parameter on the limiting current density separately (data not shown here). Therefore, it can be concluded that changes in the concentration of electroactive species and diffusivity were the most influential parameters in the reduction of the limiting current density with higher salt concentrations.

For corrosion of carbons steels in CO_2-saturated aqueous solutions, the following three equations are commonly proposed as the cathodic reactions:[24]

$$2H^+ + 2e^- \rightarrow H_2 \text{ (H}^+ \text{ reduction)} \quad (3)$$

$$2H_2CO_3 + 2e^- \rightarrow H_2 + 2HCO_3^- \text{ (direct reduction of carbonic acid)} \quad (4)$$

$$2H_2O + 2e^- \rightarrow H_2 + 2OH^- \text{ (water reduction)} \quad (5)$$

The H^+ reduction (Reaction (3)) is the dominant cathodic reaction at pH lower than 4. The carbonic acid direct reduction (Reaction (4)) becomes important at pH > 5.[18] However, recent works[25–27] have shown that the direct reduction of carbonic acid may not happen at all and that contribution of carbonic acid to the overall corrosion process is by acting as a source of H^+ for Reaction (3). This is called “buffering

effect".[25,28,29] Finally, the water reduction (Reaction (5)) becomes important at P_{CO_2}<< 1 and pH > 5.[24] Thus, under the experimental conditions used in this study the H^+ reduction was the main cathodic reduction reaction.

It seems from the potentiodynamic sweeps that the charge-transfer controlled cathodic current was retarded with increasing NaCl concentration. This suggests that the H^+ reduction was hindered by the presence of more salt in the solution. Figure 6 shows the reaction order for the cathodic reaction at three different potentials.

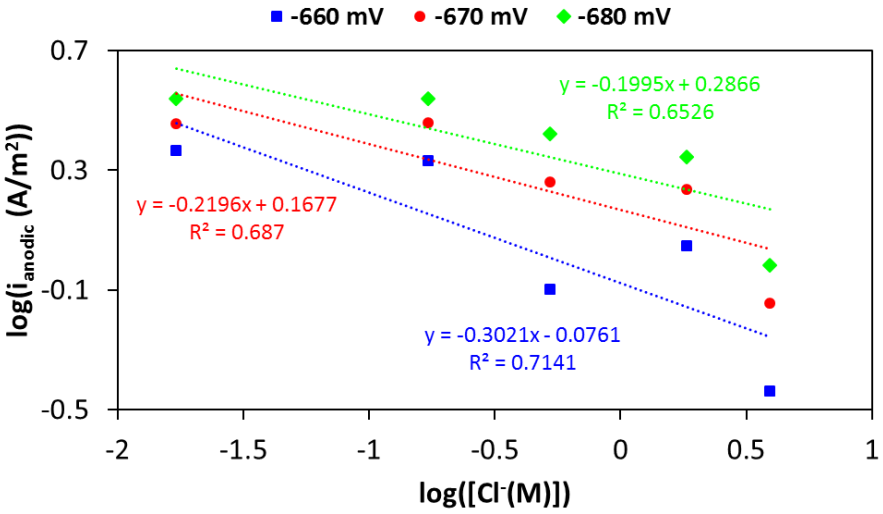

Figure 6: The steady-state charge-transfer controlled cathodic current density vs. chloride concentration at potentials: -660, -670, -680 mV vs. Ag/AgCl

The average reaction order determined from Figure 6 is -0.24. However, the accuracy of this number is questionable because it is possible that the salt concentration did not have any effect on the charge-transfer controlled cathodic current (the reaction rate of H^+ reduction) and its apparent decrease with higher NaCl concentrations was due to the retardation of the anodic current that masked the charge-transfer zone. Further investigations will be performed in near future at lower temperatures to address this issue comprehensively. The water reduction reaction occurred at potentials lower than -0.9 V vs. Ag/AgCl was not affected by the salt concentration.

Effect of salt concentration on anodic reaction

Generally, the overall anodic reaction for dissolution of carbon steels in aqueous solutions is shown by the following reaction:

$$Fe_{(s)} \rightarrow {Fe^{2+}}_{(aq)} + 2e^- \text{ (iron oxidation)} \quad (5)$$

However, Reaction (5) proceeds through different pathways depending on the nature of the solution and the steel surface microstructure. A generally accepted mechanism for dissolution of iron in acidic aqueous solutions in the absence of halides such as chloride is suggested by Bockris *et al.*[30] and Kelly[31] as follows:

$$Fe + H_2O \rightleftharpoons Fe(H_2O)_{ads} \text{ (adsorption of water molecules)} \quad (6)$$

$$Fe(H_2O)_{ads} \rightleftharpoons Fe(OH^-)_{ads} + H^+ \text{ (dissociation of water molecules)} \quad (7)$$

$$Fe(OH^-)_{ads} \rightleftharpoons (FeOH)_{ads} + e^- \text{ (formation of surface intermediate)} \quad (8)$$

$$(\mathrm{FeOH})_{\mathrm{ads}} \xrightarrow{\mathrm{RDS}} (\mathrm{FeOH})^{+} + \mathrm{e}^{-} \text{ (dissolution of iron)} \quad (9)$$

$$\mathrm{FeOH}^{+} + \mathrm{H}^{+} \rightleftharpoons \mathrm{Fe}^{2+} + \mathrm{H_2O} \text{ (decomplexation of ferrous ion)} \quad (10)$$

In the Bockris-Kelly[30,31] mechanism, the hydroxyl ion from dissociation of water molecules participates directly in the iron dissolution process. The rate-determining step (RDS) in this mechanism is Reaction (9), which its rate relies on the surface coverage of electrode with $FeOH_{ads}$. However, in the presence of chloride ions (or other halides), it is believed that there is a competition between chloride and hydroxyl ions for being adsorbed on the surface. Hackerman and McCafferty[32] have shown that the adsorption of chloride prevails over hydroxyl adsorption at high chloride concentrations and low pH. Lorenz *et al.*[33] proposed the mechanism below for iron dissolution in the presence of chloride:

$$\mathrm{Fe} + \mathrm{H_2O} \rightarrow \mathrm{Fe(H_2O)_{ads}} \text{ (adsorption of water molecules)} \quad (11)$$

$$\mathrm{Fe(H_2O)_{ads}} + \mathrm{Cl}^{-} \rightarrow \mathrm{FeCl^{-}_{ads}} + \mathrm{H_2O} \text{ (adsorption of chloride)} \quad (12)$$

$$\mathrm{FeCl^{-}_{ads}} + \mathrm{OH}^{-} \xrightarrow{\mathrm{RDS}} \mathrm{FeOH}^{+} + \mathrm{Cl}^{-} + 2\mathrm{e}^{-} \text{ (adsorption of hydroxyl/dissolution of iron)} \quad (13)$$

Followed by Reaction (10). Burstein and Davies[34] hypothesized that iron directly reacts with chloride, following in parallel with the Bockris-Kelly[30,31] mechanism:

$$Fe + Cl^{-} \rightarrow FeCl_{ads} + e^{-} \text{ (dissolution of iron)} \quad (14)$$

$$FeCl_{\mathrm{ads}} + \mathrm{OH}^{-} \xrightarrow{\mathrm{RDS}} \mathrm{Fe}OH_{ads} + \mathrm{Cl}^{-} \text{ (competitive adsorption of hydroxyl)} \quad (15)$$

The RDS for both Lorenz *et al.*[33] and Burstein and Davies[34] mechanisms is similar. Based on the both mechanisms, the reaction order for iron dissolution with respect to chloride should be -1.

The potentiodynamic sweeps in Figure 5 show that the anodic current was decelerated with increasing NaCl concentration. This confirms that the reaction order for iron dissolution with respect to chloride was negative. Figure 7 shows that for NaCl concentrations lower than 3 wt.% ($\log([Cl^{-}(M)]) = -0.28$), the average reaction order was 0.24. For NaCl concentrations greater than 3 wt.%, the average reaction order was -0.64. According to the mechanisms of iron dissolution in the presence of chloride, the changes in the anodic current can be related to the adsorption of chloride on the surface. At NaCl concentrations lower than 3 wt.%, the adsorption of chloride was not influential in the anodic dissolution of iron. Contrarily, at NaCl concentrations greater than 3 wt.% the adsorption of chloride dominates over the hydroxyl adsorption and the anodic current was retarded.

Similar values have been reported in the literature for the reaction order of iron dissolution with respect to chloride concnetration.[5,32,35] However, there have been studies that reported positive reaction orders.[7,9,36,37] When reporting a reaction order, one should pay attention to the range of Cl^{-} and H^{+} concentrations and the chosen overpotential. For example, Zeng *et al.*[7] reported a reaction order of 0.5 at pH around 4 and high overpotentials. However, at their chosen overpotential, the anodic current was in the pseudo-passive or passive regions, which makes the reported reaction order unreliable because the reaction order should be defined for the charge-transfer controlled region. Therefore, depending on the choice of parameters, different reaction orders can be reported for iron dissolution with respect to chloride concentration.

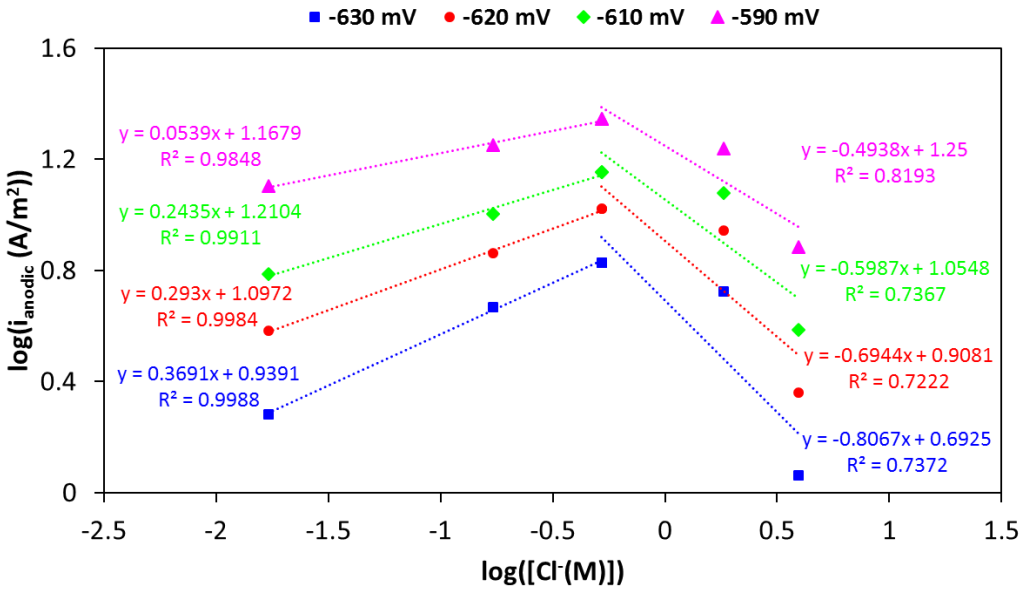

Figure 7: The steady-state anodic current density vs. chloride concentration at potentials: -630, -620, -610 and -590 mV vs. Ag/AgCl

Effect of salt concentration on overall corrosion process

The potentiodynamic sweeps in Figure 5 show that the corrosion rate decreased as a function of NaCl concentration, which is in line with the weight loss results. The decrease in the corrosion rate is attributed to deceleration in the rates of both anodic and cathodic reactions. Figure 5 shows that the limiting current density increased with an increase in NaCl concentration from 0.1 wt% to 1 wt.% and then decreased significantly by further increase in NaCl concentration, a similar trend observed for the corrosion rate (Figure 4) and the calculated H^+ concentration profile (Figure 3). This means that the mass transfer of electroactive species, mainly H^+, from the bulk to the surface–measured as the liming current density–controlled the rate of corrosion process. Therefore, the decrease in the corrosion rate with the addition of NaCl concentration was predominantly due to the decrease in the limiting current density.

EIS results

Figure 8 shows the impedance diagrams at OCP for different NaCl concentrations. The frequencies shown in Figure 8 (A) are the characteristic frequencies ($f = 1/2\pi RC$). A depressed capacitive semicircle in the high to the medium frequency ranges and an inductive loop in the low frequency range can be observed in the Nyquist plots (Figure 8 (A)). The diameter of the depressed capacitive semicircle indicates the resistance to charge-transfer controlled reactions, which is inversely proportional to the corrosion rate. The presence of an inductive loop is usually associated with the relaxation (the delay in the response of a system after an external perturbation[38]) of adsorbed iron intermediate species such as $Fe(OH)_{ads}$ on the surface.[39–41] However, Zeng *et al.*[7] and das Chagas Almeida *et al.*[40] reported that the inductive loop was not observed when the solution was sparged with a neutral gas. That is, the inductive loop is related to the dissolved CO_2 in the solution.

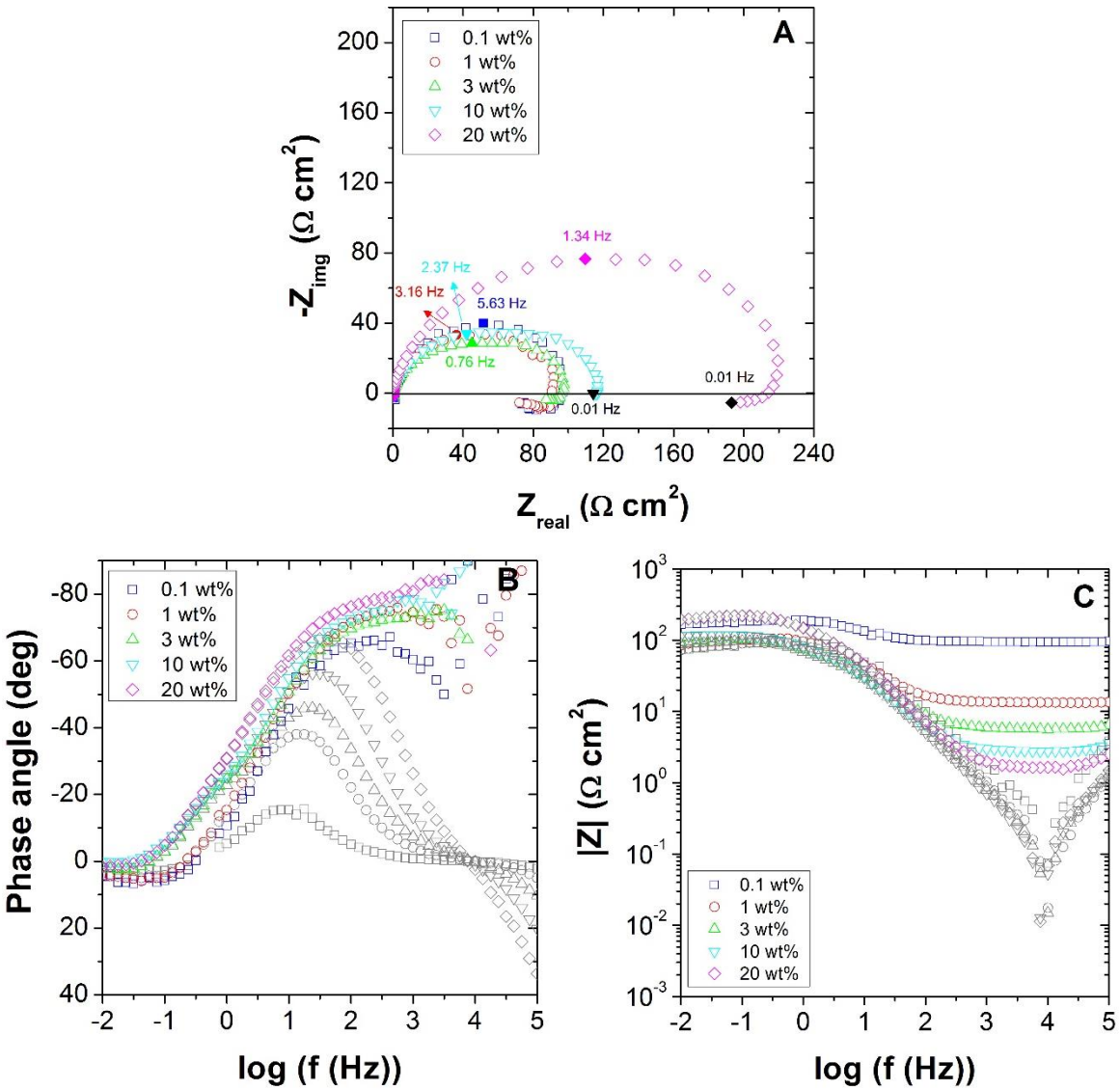

Figure 8: Impedance data in CO_2-saturated solutions (autogenous pH) with different NaCl concentrations at OCP, 30°C, 1 bar total pressure, and 1000 rpm RCE rotational speed; (A) Nyquist (all spectra are shifted to $Z_{real} = 0$ for a better comparison), (B) Modified Bode phase (the gray points are without correction for the solution resistance), and (C) Bode magnitude plots

The gray data points in Figure 8 (B) are phase angles (degree) without correction for the solution resistance ($\varphi = 180/\pi \cdot tan^{-1}(Z_{img}/Z_{real})$). On the other hand, the colored data points are phase angles (degree) with correction for the solution resistance ($\varphi = 180/\pi \cdot tan^{-1}(\frac{Z_{img}}{Z_{real}-R_s})$). The gray points in Figure 8 (C) are the impedance magnitude (Ω·cm^2) without correction for the solution resistance. However, the colored data are corrected for the solution resistance ($|Z| = \sqrt{((Z_{real} - R_s)^2 + {Z_{img}}^2)}$).[42] Both Figure 8 (B and C) show that the data points at frequencies higher than 10000 are noisy because the experiments were not stable at these frequencies. Therefore, these data points were not used in the modeling part discussed later in the text.

The modified phase angle plots show that the phase angle in the medium frequency range increased with increasing NaCl concentration. This means that the metal/electrolyte interface exhibited more

capacitive behavior at higher NaCl concentrations, which may be attributed to the adsorption of chloride intermediate species on the surface. The dispersion in the phase angles at high frequencies are because of noises during the measurements which could be spotted when the phase angle was corrected for the solution resistance. In a similar study, Eliyan *et al.* [9,10] observed an increase in the peak's height in the Bode phase plot with higher NaCl contents. They related this trend to the formation of a mixed layer of $FeCO_3$ and FeC_3 on the surface of electrode. However, as mentioned earlier, no $FeCO_3$ was detected on the surface of the specimen in this study, which leaves only the formation of FeC_3. The latter cannot be the reason for the increase in the peak's height because with increasing NaCl concentration the corrosion rate decreased, which means less FeC_3 formed on the surface.

The Randles circuit shown in Figure 9 was used to model the experimental EIS data. Although it might not be the best representative of the metal/solution interface, since it captures the data points in the high frequency range, it is adequate for determining the charge transfer resistance and the double-layer capacitance. The fitted circuit parameters are listed in Table 4.

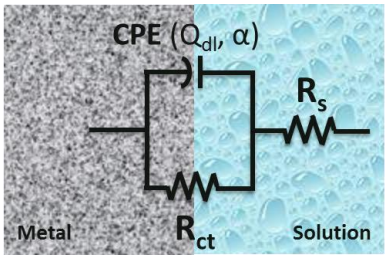

Figure 9: Randles equivalent circuit with a constant phase element (CPE) used for fitting the experimental impedance spectra

Table 4: Best-fit equivalent circuit parameters for different NaCl concentrations

NaCl (wt.%)	R_s (Ω·cm^2)	Q_{dl} (μF·cm^{-2}·s$^{α-1}$)	α	R_{ct} (Ω·cm^2)
0.1	100.8	8.37E-4	0.77	100.7
1	28.6	1.06E-3	0.81	85.5
3	4.8	9.99E-4	0.81	66.6
10	2.7	9.37E-4	0.84	84.7
20	1.6	5.43E-4	0.87	176.9

The double-layer capacitance (C_{dl}) can be calculated using Brug *et al.*[43] equation:

$$C_{dl} = Q_{dl}^{\frac{1}{\alpha}}\left(\frac{1}{R_s} + \frac{1}{R_{ct}}\right)^{1-\frac{1}{\alpha}} \quad (16)$$

where C_{dl} is in μF/cm^2, Q_{dl} is a constant representative for the CPE in μF·cm^{-2}·s$^{α-1}$, α is a dimensionless parameter varies between zero and one, R_s is the solution resistance in Ω·cm^2, and R_{ct} is the charge transfer resistance in Ω·cm^2. The double-layer capacitance on a bare metal is typically in the range of 10 to 50 μF/cm^2.[44] However, as shown in Figure 10, the measured values were one order of magnitude higher than the typical range. This is because of a rough surface caused by the formation of Fe_3C matrix on the surface of the electrode during the corrosion process. A higher surface roughness results in a larger surface area that leads to a higher double-layer capacitance.[45] Figure 10 depicts the variation in the double-layer capacitance with increasing NaCl concentration. The capacitance of the double layer first increased and then decreased with higher NaCl concentrations, similar to the trend observed for the corrosion rate. At higher NaCl concentrations, the thickness of the Fe_3C matrix becomes smaller because of a lower corrosion rate. Therefore, the surface roughness will be smaller that results in a smaller double-layer capacitance.

From another perspective, according to the Helmholtz double layer model, the capacitance of double layer can be calculated from the following equation:

$$C_{dl} = \frac{\varepsilon_0 \varepsilon}{\delta} \tag{17}$$

where, C_{dl} is the capacitance of Helmholtz double layer per unit surface area in F/cm^2, ε_0 is the permittivity of vacuum (8.8542E-14 F/cm), ε is the relative permittivity of electrolyte (dimensionless) and δ is the thickness of Helmholtz double layer in cm.[44,46] Equation (17) is for a planar electrode or cylindrical electrode with a radius >> δ.[46]

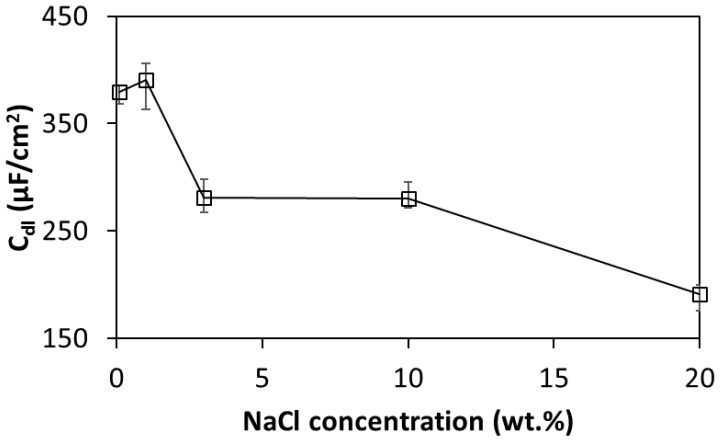

Figure 10: Changes in the double-layer capacitance with NaCl concentration

The decrease in the double-layer capacitance with increasing NaCl concentration could be because of an increase in the thickness of the double layer or a decrease in the relative dielectric of electrolyte.[47] However, Brown *et al.*[48] reported that the thickness of the double layer at the surface of a silica electrode decreased as NaCl concentration in water was increased from zero to 0.12 M (~0.7 wt.%). If their result is correct and expandable to higher NaCl concentrations, this means that the electrolyte permittivity should decrease sharply with higher NaCl concentration.

Figure 11 compares the charge transfer resistance obtained with EIS and LPR. The charge transfer resistance obtained with LPR is comparable to that measured with EIS because the frequency corresponding to the LPR measurements (0.0125 Hz) is almost the same as that used for determining the charge transfer resistance from the Nyquist diagrams. The charge transfer obtained by EIS is lower than the LPR charge transfer probably because LPR cannot distinguish between the faradaic and non-faradaic processes and the measured charge transfer is a combination of all processes that affect the charge transfer including adsorption of intermediate species on the surface. However, EIS has this advantage over LPR and other DC techniques that the resistance related exactly to the charge transfer process can be separated from that related to other processes such as adsorption of intermediate species (inductive loop).[49]

The charge transfer resistance obtained with EIS decreased with increasing NaCl concentration from 0.1 to 3 wt.%, and then increased continuously by further increase in NaCl concentration. In similar studies, Eliyan *et al.*[9,10] reported a decrease in the charge transfer resistance with increasing NaCl concentration up to 80 g/L (~7 wt.%). However, higher NaCl concentrations were not examined in their studies.

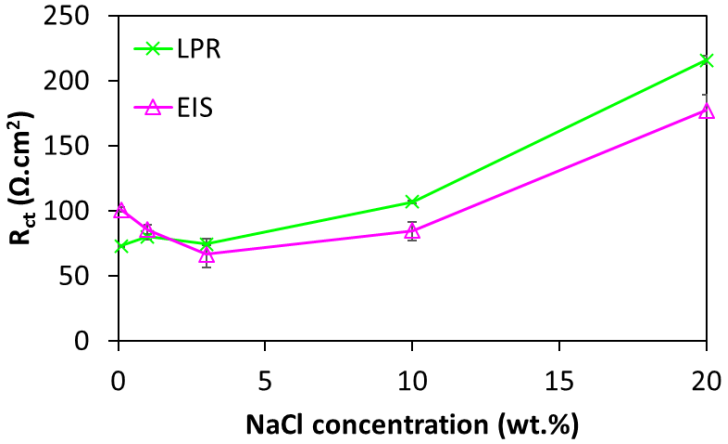

Figure 11: Comparison of charge transfer resistance obtained with LPR and EIS

Figure 12 compares the corrosion rates measured with weight loss, LPR and EIS at different NaCl concentrations. The corrosion rate measured with EIS had a similar trend to those measured with weight loss and LPR. However, the corrosion rates estimated by EIS were larger.

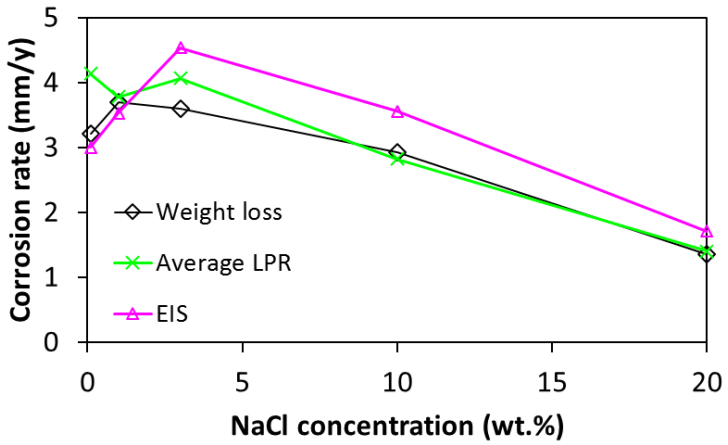

Figure 12: Comparison of corrosion rate measured with weight loss, LPR and EIS

CONCLUSIONS

The effect of salt concentration (ionic strength) on uniform CO_2 corrosion of carbon steel was investigated by conducting weight loss and electrochemical experiments in CO_2-saturated solutions at different NaCl concentrations ranging from zero to 20 wt.%, 30°C, autogenous pH, and 1 bar total pressure. The following are major conclusions found in this study:

1. With the addition of NaCl to CO_2-saturated DI water, the pH of solution decreased because of an increase in the activity coefficient of H^+, while H^+ concentration decreased due to salting out effect.
2. The corrosion rate reached a maximum at 1 wt.% NaCl and then decreased continuously by further increase in NaCl concentration.
3. The key change in the potentiodynamic sweeps due to an increase in NaCl concentration was the reduction of the liming current density. Moreover, the anodic current was retarded by increasing NaCl concentration. No decisive conclusion could be made about the cathodic current in the charge-transfer controlled region.

4. The changes in the concentration and diffusion coefficient of electroactive species were the most influential parameters in the reduction of the limiting current density with higher salt concentrations.
5. Mass transfer of electroactive species, mainly H^+, from the bulk to the surface–measured as the liming current density– controlled the rate of corrosion process. The decrease in the corrosion rate with the addition of NaCl concertation was predominantly due to the decrease in the limiting current density.
6. EIS results confirmed the weight loss and the potentiodynamic results. EIS data showed that the charge transfer resistance increased with increasing NaCl concentration, while the double-layer capacitance decreased.
7. The decrease in the capacitance of the double layer was attributed to a lower surface roughness at higher NaCl concentrations.

ACKNOWLEDGEMENTS

The authors would like to gratefully acknowledge the constructive help of Dr. Bernard Tribollet. The authors are greatly thankful to the following companies for their financial support: Anadarko, Baker Hughes, BP, Chevron, CNOOC, ConocoPhillips, DNV GL, ExxonMobil, M-I SWACO (Schlumberger), Multi-Chem (Halliburton), Occidental Oil Company, PTT, Saudi Aramco, SINOPEC (China Petroleum), and TOTAL.

REFERENCES

1. Igunnu, E.T., and G.Z. Chen, *Int. J. Low-Carbon Technol.* 9 (2014): pp. 157–177.
2. "Reclamation Managing Water in the West: Oil and Gas Produced Water Management and Beneficial Use in the Western United States" (US Department of the Interior Bureau of Reclamation, 2011).
3. SPE International, "Produced Oilfield Water," PetroWiki (2018), https://petrowiki.org/Produced_oilfield_water (Sep. 10, 2018).
4. Breit, G.N., "USGS Produced Waters Database" (U.S. Department of the Interior, 2002).
5. Fang, H., "Low Temperature and High Salt Concentration Effects on General CO_2 Corrosion for Carbon Steel," Master's thesis, Ohio University, 2006.
6. Fang, H., S. Nesic, B. Brown, and S. Wang, "General CO_2 Corrosion in High Salinity Brines" (NACE International, 2006).
7. Zeng, Z., R. s. Lillard, and H. Cong, *CORROSION* 72 (2016): pp. 805–823.
8. Han, J., J.W. Carey, and J. Zhang, *J. Appl. Electrochem.* 41 (2011): pp. 741–749.
9. Eliyan, F.F., F. Mohammadi, and A. Alfantazi, *Corros. Sci.* 64 (2012): pp. 37–43.
10. Eliyan, F., and A. Alfantazi, *J. Appl. Electrochem.* 42 (2012): pp. 233–248.
11. Liu, Q.Y., L.J. Mao, and S.W. Zhou, *Corros. Sci.* 84 (2014): pp. 165–171.
12. Madani Sani, F., A. Afshar, and M. Mohammadi, *Int. J. Electrochem. Sci.* 11 (2016): pp. 3887–3907.
13. Rogers, P.S.Z., and K.S. Pitzer, *J. Phys. Chem. Ref. Data* 11 (1982): pp. 15–81.
14. Hinds, G., P. Cooling, A. Wain, S. Zhou, and A. Turnbull, *CORROSION* 65 (2009): pp. 635–638.
15. Fontana, M.G., *Corrosion Engineering* (Tata McGraw-Hill, 2005).
16. Pitzer, K.S., *J. Phys. Chem.* 77 (1973): pp. 268–277.
17. Wang, P., A. Springer, and R.D. Young, *Fluid Phase Equilibria* 222–223 (2004): pp. 11–17.
18. Nesic, S., J. Postlethwaite, and S. Olsen, *CORROSION* 52 (1996): pp. 280–294.
19. Gray, L.G.S., B.G. Anderson, M.J. Danysh, and P.R. Tremaine, "Mechanisms of Carbon Steel Corrosion in Brines Containing Dissolved Carbon Dioxide At PH 4," in NACE Int. (1989), p. No. 464.
20. Gray, L.G.S., B.G. Anderson, M.J. Danysh, and P.R. Tremaine, "Effect of PH and Temperature on the Mechanism of Carbon Steel Corrosion by Aqueous Carbon Dioxide," in NACE Int. (1990), p. No. 40.

21. Ogundele, G.I., and W.E. White, *Corrosion* 42 (1986): pp. 398–408.
22. George, K.S., and S. Nešić, *CORROSION* 63 (2007): pp. 178–186.
23. Eisenberg, M., C.W. Tobias, and C.R. Wilke, *J. Electrochem. Soc.* 101 (1954): pp. 306–320.
24. Nesic, S., R. Nyborg, A. Stangeland, and M. Nordsveen, "A Mechanistic Modeling for CO_2 Corrosion with Protective Iron Carbonate Films" (NACE International, 2001), p. No. 01040.
25. Remita, E., B. Tribollet, E. Sutter, V. Vivier, F. Ropital, and J. Kittel, *Corros. Sci.* 50 (2008): pp. 1433–1440.
26. Tran, T., B. Brown, and S. Nesic, "Corrosion of Mild Steel in an Aqueous CO_2 Environment – Basic Electrochemical Mechanisms Revisited," in NACE Int. (Dallas, TX, 2015), p. No. 5671.
27. Kahyarian, A., B. Brown, and S. Nesic, "Mechanism of CO_2 Corrosion of Mild Steel: A New Narrative" (NACE International, 2018), https://www.onepetro.org/conference-paper/NACE-2018-11232 (Dec. 1, 2018).
28. Hurlen, T., S. Gunvaldsen, R. Tunold, F. Blaker, and P.G. Lunde, *J. Electroanal. Chem. Interfacial Electrochem.* 180 (1984): pp. 511–526.
29. Linter, B.R., and G.T. Burstein, *Corros. Sci.* 41 (1999): pp. 117–139.
30. Bockris, J.O., D. Drazic, and A.R. Despic, *Electrochimica Acta* 4 (1961): pp. 325–361.
31. Kelly, E.J., *J. Electrochem. Soc.* 112 (1965): pp. 124–131.
32. McCafferty, E., and N. Hackerman, *J. Electrochem. Soc.* 119 (1972): pp. 999–1009.
33. Lorenz, W.J., H. Yamaoka, and H. Fisher, *Ber Bunsenges Phys Chem* 67 (1963): pp. 932–943.
34. Burstein, G.T., and D.H. Davies, *Corros. Sci.* 20 (1980): pp. 1143–1155.
35. Darwish, N.A., F. Hilbert, W.J. Lorenz, and H. Rosswag, *Electrochimica Acta* 18 (1973): pp. 421–425.
36. Chin, R.J., and K. Nobe, *J. Electrochem. Soc.* 119 (1972): pp. 1457–1461.
37. Kuo, H.C., and K. Nobe, *J. Electrochem. Soc.* 125 (1978): pp. 853–860.
38. Ilgenfritz, G., "Theory and Simulation of Chemical Relaxation Spectra," in Chem. Relax. Mol. Biol., eds. I. Pecht, and R. Rigler (Berlin, Heidelberg: Springer Berlin Heidelberg, 1977), pp. 1–42, https://doi.org/10.1007/978-3-642-81117-3_1 (Sep. 30, 2018).
39. Zhang, G.A., and Y.F. Cheng, *Corros. Sci.* 51 (2009): pp. 87–94.
40. das Chagas Almeida, T., M.C.E. Bandeira, R.M. Moreira, and O.R. Mattos, *Corros. Sci.* 120 (2017): pp. 239–250.
41. Ma, H.Y., C. Yang, G.Y. Li, W.J. Guo, S.H. Chen, and J.L. Luo, *CORROSION* 59 (2003): pp. 1112–1119.
42. Orazem, M.E., and B. Tribollet, *Electrochemical Impedance Spectroscopy*, 2 edition (Hoboken, New Jersey: Wiley, 2017).
43. Brug, G.J., A.L.G. van den Eeden, M. Sluyters-Rehbach, and J.H. Sluyters, *J. Electroanal. Chem. Interfacial Electrochem.* 176 (1984): pp. 275–295.
44. Orazem, M.E., and B. Tribollet, "Electrochemistry," in Electrochem. Impedance Spectrosc. (Wiley-Blackwell, 2008), pp. 73–96.
45. Thomas, G.M., "Does Controlled Roughing of a Surface Increase Its Capacitance?," Bachelor's, Worcester Polytechnic Institute, 2012.
46. Wang, H., and L. Pilon, *J. Phys. Chem. C* 115 (2011): pp. 16711–16719.
47. Farag, A.A., and M.A. Hegazy, *Corros. Sci.* 74 (2013): pp. 168–177.
48. Brown, M.A., A. Goel, and Z. Abbas, *Angew. Chem. Int. Ed.* 55 (2016): pp. 3790–3794.
49. Lorenz, W.J., and F. Mansfeld, *Corros. Sci.* 21 (1981): pp. 647–672.